M.A.L. Nicolelis (Ed.)
Progress in Brain Research, Vol. 130

CHAPTER 3

Overcoming the limitations of correlation analysis for many simultaneously processed neural structures

Luiz A. Baccalá [1,*] and Koichi Sameshima [2]

[1] *Telecommunications and Control Enginering Department, Escola Politécnica, Av. Prof. Luciano Gualberto, Trav. 3, #158, University of São Paulo, São Paulo, SP, CEP 05508-900, Brazil*
[2] *Disc. Medical Informatics and Functional Neurosurgery Laboratory, School of Medicine, University of São Paulo, São Paulo, Brazil*

Introduction

Despite modern methods in molecular biology, neuroanatomy, and functional imaging, monitoring electric signals from neuronal depolarization remains important when evaluating the functional aspects of both normal and pathological neural circuitry. Correlation methods still rank popular and are extensively used to analyze the functional interaction in the electroencephalogram (EEG), the magnetoencephalogram, local field potentials and more recently, in simultaneously recorded single- and multiunit activity of many structures (tens to hundreds at a time). This last item has deserved increasing attention due to its potential in bridging the gap between the study of isolated single neurons and the understanding of encoding and processing of information by neuronal populations (Eichenbaum and Davis, 1998; Nicolelis, 1998).

A host of other analytical techniques have emerged, some employing information theoretic rationales by assessing mutual information (Yamada et al., 1993; Rieke et al., 1997; Brunel and Nadal, 1998) or interdependence between signal pairs (Schiff et al., 1996; Arnhold et al., 1999), while others are extensions of spectral analysis/coherence analysis (Glaser and Ruchkin, 1976; Duckrow and Spencer, 1992; Christakos, 1997; Rosenberg et al., 1998). Despite these advances, a large fraction of neuroscientists still chiefly rely on the cross-correlation between the activity of pairs of neural structures to infer their functionality.

Like cross-correlation, all of these methods are in one way or another restricted in their calculations to using just the signal of two structures at a time. In this article, we show that it is not only possible but also desirable to analyze more than two structures simultaneously. Furthermore, we show also that effective structural inference is only possible if simultaneous signals from many (representative) structures are jointly analyzed.

To handle many simultaneous structures, we employ the recently introduced notion of *partial directed coherence* (PDC). This is a novel frequency domain approach for simultaneous multichannel data analysis based on Granger causality that employs multivariate auto-regressive (MAR) models for computational purposes (Baccalá and Sameshima, 1999). We review PDC in Section 2 and illustrate its usefulness via toy linear models simulating multi-electrode EEG measurements in Section 3, where we contrast

* Corresponding author: Luiz A. Baccalá, Telecommunications and Control Enginering Department, Escola Politécnica, Av. Prof. Luciano Gualberto, Trav. 3, #158, University of São Paulo, São Paulo, SP, CEP 05508-900, Brazil. E-mail: baccala@lcs.poli.usp.br

it to other techniques (correlation/coherence analysis). We discuss an application to experimental data in Section 4. Further examples of PDC in a single- and multi-unit activity context are available in Sameshima and Baccalá (1999).

Partial directed coherence

The concept of *partial directed coherence* is the latest development of a number of time series analysis efforts for describing how neural structures are interconnected (Baccalá and Sameshima, 1999; Sameshima and Baccalá, 1999). Its remote origin is the paper by Saito and Harashima (1981) which introduced the notion of *directed coherence* between the activity of pairs of structures. Their method allows factoring the classical coherence function (the frequency domain counterpart of correlation analysis) of a pair of structures into two 'directed coherences': one representing the *feedforward* and the other one representing the *feedback* aspects of the interaction between these two neural structures. Examples of use of pairwise directed coherence in studying the relation between Parkinson's tremor and lack of feedback in motor control are contained in Schnider et al. (1989).

In an attempt to generalize directed coherence to a context of analysis of more than two simultaneously processed structures, the so-called method of *directed transfer function* (DTF) was introduced with several equivalent variants (Franaszczuk et al., 1994; Baccalá and Sameshima, 1998; Baccalá et al., 1998). This method was applied to foci determination and to EEG studies in mesial temporal lobe seizure (Franaszczuk et al., 1994). Details on DTF are contained in Appendix A.

In their original paper, Saito and Harashima (1981) allude to a possible rationale for their method. This concept is now known as Granger causality (Granger, 1969). According to it, *an observed time series $x(n)$ Granger-causes another series $y(n)$, if knowledge of $x(n)$'s past significantly improves prediction of $y(n)$; this kind of predictability improvement is not reciprocal, i.e. $x(n)$ may Granger-cause $y(n)$ without $y(n)$ necessarily Granger-causing $x(n)$*. This lack of reciprocity is the basic property behind the determination of the direction of information flow between pairs of structures which, in turn, is the basis for decomposing classical coherence into directed feedforward and feedback coherence factors.

Following that rationale, we investigated how generalizations, like DTF, of directed coherence to N simultaneously processed structures compared to statistical tests of Granger causality for N simultaneous time series (Baccalá et al., 1998). We realized that DTF provided a physiologically interesting frequency domain picture, yet structural inference based on its computation did not always agree with the result of Granger causality tests (GCT). We could show that this was due to intrinsic aspects of DTF's definition (Baccalá and Sameshima, 1999) (see also Appendix A).

Because Granger causality is a more fundamental concept than the ad hoc generalization represented by DTF, we went on to introduce the notion of partial directed coherence (Baccalá and Sameshima, 1999). This new structural connectivity estimator relies on the simultaneous processing of $N \geq 2$ time series and is able to expose a frequency domain picture of the feedforward and feedback interactions between each and every pair of structures within the set of N simultaneously processed signals. Perhaps more importantly, PDC reflects Granger causality closely by paralleling the definition of Granger causality test estimators.

The main preliminary ingredient of both PDC and GCT (and of DTF as well, but in a fundamentally different way) is their practical use of multivariate autoregressive models as exemplified for $N = 3$ simultaneously monitored structures in the model

$$\begin{bmatrix} x_1(n) \\ x_2(n) \\ x_3(n) \end{bmatrix} = \sum_{r=1}^{p} \begin{bmatrix} a_{11}(r) & a_{12}(r) & a_{13}(r) \\ a_{21}(r) & a_{22}(r) & a_{23}(r) \\ a_{31}(r) & a_{32}(r) & a_{33}(r) \end{bmatrix} \times \begin{bmatrix} x_1(n-r) \\ x_2(n-r) \\ x_3(n-r) \end{bmatrix} + \begin{bmatrix} w_1(n) \\ {}_2(n) \\ w_3(n) \end{bmatrix} \quad (1)$$

In this model, $x_1(n)$ depends on its own past values $x_1(n-r)$ through the coefficients $a_{11}(r)$ while, for example, $x_1(n)$'s dependence on the past values of the other series like $x_2(n-r)$ is through the $a_{12}(r)$ coefficients. As such, the time series $x_2(n)$ only Granger-causes $x_1(n)$ if we can statistically show that $a_{12}(r) \neq 0$ for some values of r. Or equivalently,

rejecting the null hypothesis of $a_{ij}(r) = 0$ means that $x_j(n)$ does Granger-cause $x_i(n)$.

The partial directed coherence from series j to series i, at frequency f can be defined as

$$\pi_{ij}(f) = \frac{\bar{a}_{ij}(f)}{\sqrt{\bar{\boldsymbol{a}}_j(f)^H \bar{\boldsymbol{a}}_j(f)}} \tag{2}$$

where

$$\bar{a}_{ij}(f) = \begin{cases} 1 - \sum_{r=1}^{p} a_{ij}(r) e^{-j2\pi f r}, & \text{if } i = j \\ -\sum_{r=1}^{p} a_{ij}(r) e^{-j2\pi f r}, & \text{otherwise} \end{cases} \tag{3}$$

and $\bar{\boldsymbol{a}}_j(f)$ is the vector

$$\bar{\boldsymbol{a}}_j(f) = \begin{bmatrix} \bar{a}_{1j}(f) \\ \vdots \\ \bar{a}_{Nj}(f) \end{bmatrix} \tag{4}$$

Because of its dependence on $a_{ij}(r)$ in Eq. 3, the nullity of $\pi_{ij}(f)$ at a given frequency implies lack of Granger causality from $x_j(n)$ to $x_i(n)$ at that frequency. PDC is, therefore, a direct frequency domain counterpart of GCT.

Though further details on PDC are contained elsewhere (Baccalá and Sameshima, 1999), a compact summary is available at Appendix A together with its relation to DTF. Methods of MAR model fitting are reviewed elsewhere (Marple, 1987). In the next section, we discuss some examples of PDC's application contrasting it to other techniques.

Illustrative simulations

To provide objective comparisons of PDC with other techniques, we use time series generated from known linear toy models. In this case, exact theoretical calculations of pairwise cross-correlation, classical coherence, DTF and PDC can be made and allow exposing all the relative methodological merits of each approach while avoiding possible pitfalls of experimental signals collected from neural systems with unknown structure. The use of toy models is further motivated by the desire to investigate possible structural inference impairments when simultaneously processing fewer than the N structures important to the dynamics.

The first toy model example, mimicking local field potential measurements along hippocampal structures, is represented by the following set of linear difference equations with $N = 7$ structures:

Model I

$$\begin{aligned}
x_1(n) &= 0.95\sqrt{2}x_1(n-1) - 0.9025x_1(n-2) \\
&\quad + w_1(n) \\
x_2(n) &= -0.5x_1(n-1) + w_2(n) \\
x_3(n) &= 0.4x_2(n-2) + w_3(n) \\
x_4(n) &= -0.5x_3(n-1) + 0.25\sqrt{2}x_4(n-1) \\
&\quad + 0.25\sqrt{2}x_5(n-1) + w_4(n) \\
x_5(n) &= -0.25\sqrt{2}x_4(n-1) \\
&\quad + 0.25\sqrt{2}x_5(n-1) + w_5(n) \\
x_6(n) &= 0.95\sqrt{2}x_6(n-1) - 0.9025x_6(n-2) \\
&\quad + w_6(n) \\
x_7(n) &= -0.1x_6(n-2) + w_7(n)
\end{aligned}$$

with $w_i(n)$ standing for innovation noises.

These equations are designed so that $x_1(n)$ behaves as an oscillator driving the other structures, either directly or indirectly, according to the diagram in Fig. 1. Note that the interaction between $x_1(n)$ and $x_3(n)$ is both via a direct path and via an indirect route through $x_2(n)$. The dynamics of the pair $x_4(n)$ and $x_5(n)$ is designed so that they jointly represent an oscillator, whose intrinsic characteristics are due to their mutual signal feedback but which are entrained to the rest of the structure via $x_3(n)$. The signals $x_6(n)$ and $x_7(n)$ belong to a totally separate substructure where $x_6(n)$ is designed to generate oscillations at the same frequency as $x_1(n)$; $x_7(n)$ does not feedback anywhere. A sample of the signals produced in this way can be appreciated in Fig. 2.

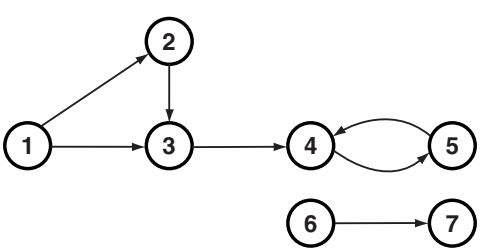

Fig. 1. Signal flow diagram for Model I.

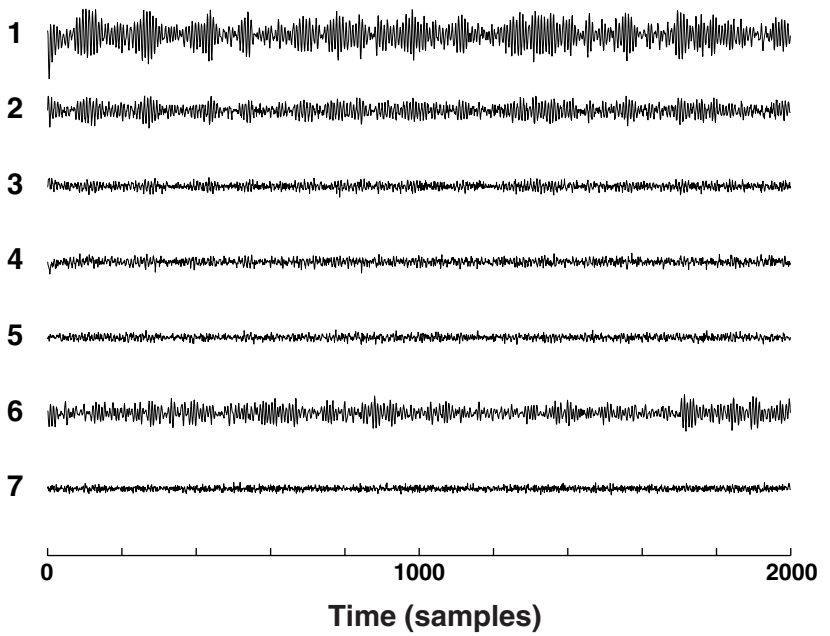

Fig. 2. Signals obtained by simulating Model I.

We begin our analysis by inspecting the theoretical pairwise cross-correlation contained in the array of plots in Fig. 3a.

Consider just the latencies and lead structures represented by the theoretical correlation maxima of Fig. 3a as summed up in Fig. 3b's diagram whose arrows are labelled with the absolute values of the latencies and originate in the leading structure. In deducing the structural relationships between the signals using this information, we may attempt to trim the diagram in Fig. 3b. This leads to several possible hypothetical structures compatible with the observed latencies such as in Fig. 3c,d. Note that structural ambiguities not only remain and but also that no conceivable trimming of Fig. 3b can possibly produce the correct solution in Fig. 1 because Fig. 3b's relation between $x_3(n)$ and $x_2(n)$ turns out inverted with respect to that in Fig. 1.

In short, this example shows that correlation information alone leads to ambiguous structural inference when considering several time series measurements simultaneously.

The results of the pairwise interaction using the theoretical DTF is depicted by dark shaded curves along the off-diagonals over a 7×7 array layout of plots of Fig. 4a. Along the shaded main diagonal of the array in Fig. 4a, we portray the power spectrum for each time series. Note the spectral similarity that characterizes all signals for this structure. To facilitate comparisons, solid-line graphs along the off-diagonals of the array depict the high pairwise classical coherences among those structures that are interconnected. Fig. 4c's schematic represents a summary of the relations described by DTF in which signal sources are labelled along the x-axis and targets along the y-axis. Thus, for instance, in Fig. 4c, an arrow leaves $x_1(n)$ and reaches $x_5(n)$ because the first column of Fig. 4a has a significant shaded area in row five. No direct reverse arrow exists as there is no dark shaded area in column 5, row 1 of Fig. 4a. In this and later graphs, thinner/dashed arrows portray weaker connections. This leads to a complex connectivity pattern in the graph describing DTF relationships (Fig. 4c). As in the case of cross-correlation, the only possible inference is, for example, that the signal in $x_1(n)$ affects all other nodes without clues as to how or through which pathway this interaction takes place. Using the same rule for associating source to target in labelling pairwise interaction using PDC, a completely distinct situation emerges in Fig. 4b where PDC calculations (dark shaded curves along the off-diagonal) lead to

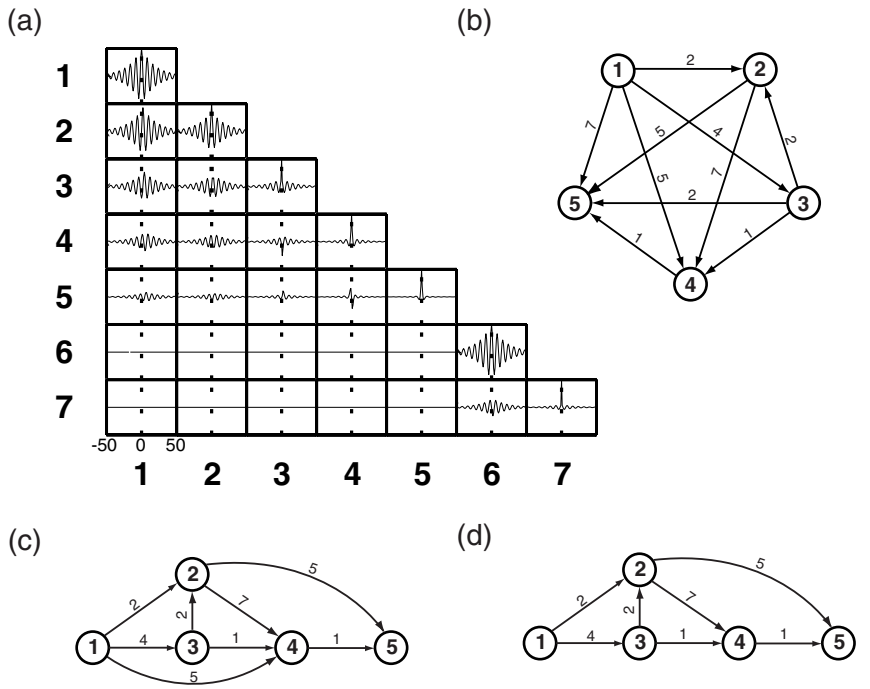

Fig. 3. The theoretical autocorrelations are shown along the main diagonal and, below it, all the theoretical cross-correlation functions are plotted (a), with the x-axis scale ranging from -50 to 50 sample points, and the y-axis is between -1 and 1. Directed graph summarizing signal propagation latency information (encoded via arrow labels) contained in the cross-correlation function (b). Two possible simplified structures compatible with the theoretically calculated latencies are shown in (c) and (d). Note that, the graph simplification from (c) to (d), the connection $1 \rightarrow 4$ (with propagation latency 5 time units) is removed because it can be explained by the pathway $1 \rightarrow 3 \rightarrow 4$ with the same total propagation latency value.

the correct structure of Fig. 4d (compare with Fig. 1).

We next slightly increase the complexity of this example by adding a feedback from $x_5(n)$ to $x_1(n)$. This is accomplished by rewriting the first equation in Model I as

$$x_1(n) = 0.95\sqrt{2}x_1(n-1) - 0.9025x_1(n-2) + 0.5x_5(n-2) + w_1(n) \quad (5)$$

in accord with the diagram of Fig. 5.

As in the previous case, the theoretical DTF is difficult to analyze (Fig. 6a,c), as opposed to PDC (Fig. 6b,d) which clearly reflects the newly added feedback. This pattern of straightforward analysis using PDC carries over to a practical simulation scenario of using 500 data points where the feedback-free situation (Fig. 7a) is easily distinguishable from that when feedback from $x_5(n)$ to $x_1(n)$ is present (Fig. 7b).

To provide some sense of the potential temporal resolution of the method, we display the time evolution of PDCs involving $x_1(n)$ and $x_5(n)$ (Fig. 8) while randomly switching the feedback on and off. Each PDC estimate comprises the use of 250 simulated data points with 50% overlap between adjacent data segments.

In comparing these examples, note that DTF's graph has arrows connecting almost all structures when the feedback is switched on (Fig. 6c); this is related to the fact that the PDC graph contains pathways (direct or indirect) that connect any two structures. Some arrows in Fig. 6c are missing ($x_2(n) \rightarrow x_1(n)$, $x_3(n) \rightarrow x_1(n)$, $x_3(n) \rightarrow x_5(n)$). Their presence would have made Fig. 6c's graph fully connected. Though corresponding to existing signal pathways, the missing arrows correspond to small (but theoretically nonzero) DTFs that reflect the weakness of the connection strength of the total pathways between structures that are far apart from one another. In fact, DTF can be interpreted as a marker for signal energy 'reachability' (see

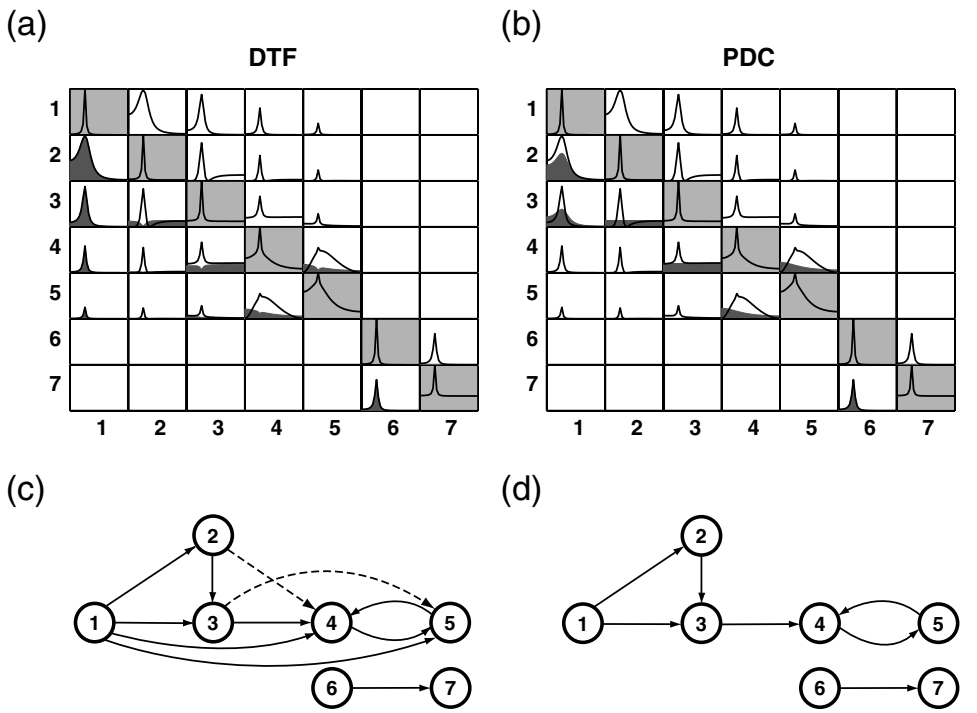

Fig. 4. Comparison between the theoretical DTF (a) (and its inferred structural interactions (c)) and the theoretical PDC results (b) (with its signal flow diagram (d)). In both cases the signal flow graphs are constructed by assigning an arrow from the source structure (x-axis) to the targets (y-axis) when dark shaded areas are significant. The spectral densities for the time series are depicted along the shaded main diagonal of the arrays. The pairwise classical coherences (solid lines) are also depicted. In all plots, the x-axis represents the normalized frequency in the 0 to 0.5 range, while the y-axis for power spectrum plots is scaled between 0 and peak value and values for the other coherence plots lie between 0 and 1.

Remark 3 in Appendix A) and must be analyzed with care. For example, examine the dip in the DTF from $x_2(n)$ to $x_3(n)$ in Figs. 4a and 6a. It coincides with the maximum of the power spectrum of both these series. Rather than mean lack of pathway connection at that frequency, this dip exemplifies (by model design) how the energy reaching a structure ($x_3(n)$) from another structure ($x_1(n)$) at one frequency may be almost exactly cancelled by the energy coming through another pathway ($x_2(n)$) due to a phase inversion in the signal.

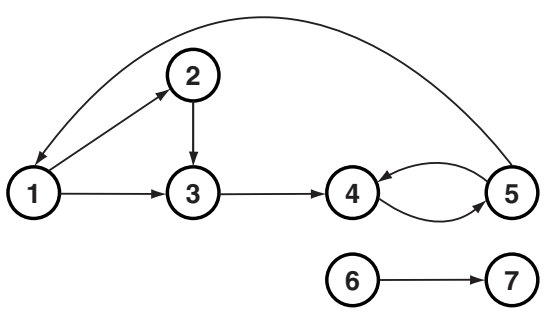

Fig. 5. Schematic diagram describing the inclusion of feedback from $x_5(n)$ to $x_1(n)$ into Model I.

To emulate scalp EEG, our second example employed

Model II

$$
\begin{aligned}
x_1(n) &= 1.8982x_1(n-1) - 0.9025x_1(n-2) \\
&\quad + w_1(n) \\
x_2(n) &= 0.9x_1(n-2) + w_2(n) \\
x_3(n) &= 0.85x_2(n-2) + w_3(n) \\
x_4(n) &= 0.82x_1(n-2) + 0.6x_6(n-3) + w_4(n) \\
x_5(n) &= -0.9x_6(n-2) + 0.4x_2(n-4) + w_5(n) \\
x_6(n) &= 0.9x_5(n-2) + w_6(n)
\end{aligned}
$$

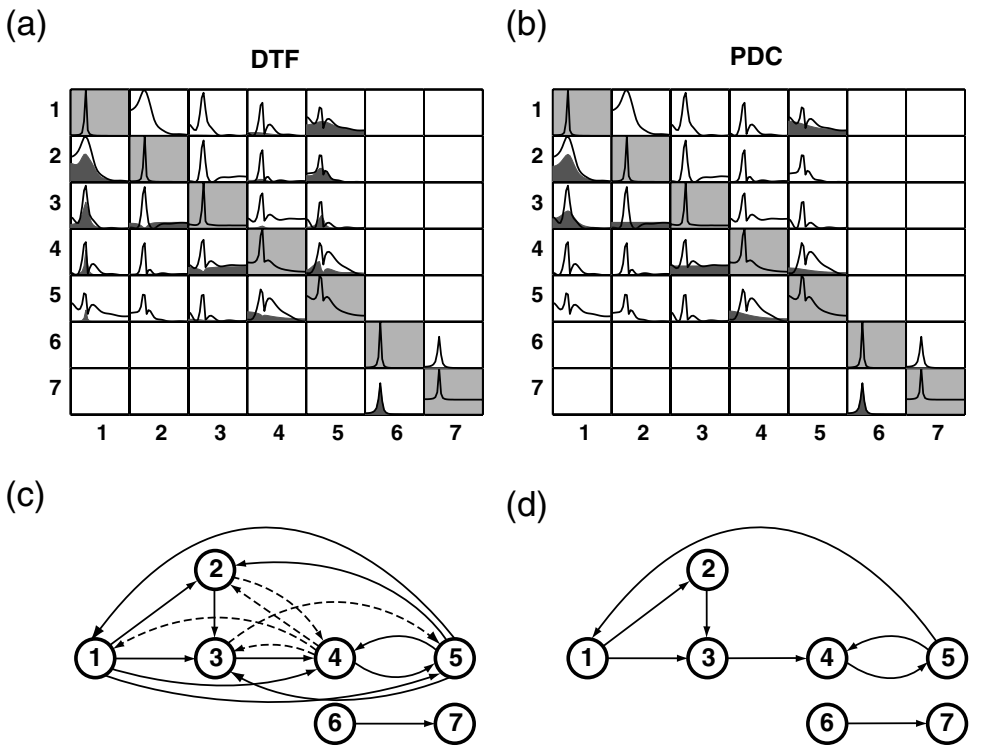

Fig. 6. Comparison between the theoretical DTF (a) (and its inferred structural interactions (c)) and the theoretical PDC results (b) (with its signal flow diagram (d)) after turning on the feedback from $x_5(n)$ to $x_1(n)$. Spectral densities for the time series are depicted along the shaded main diagonal of the arrays. The pairwise classical coherences (solid lines) are also depicted. Thin/dashed arrows portray weaker connections.

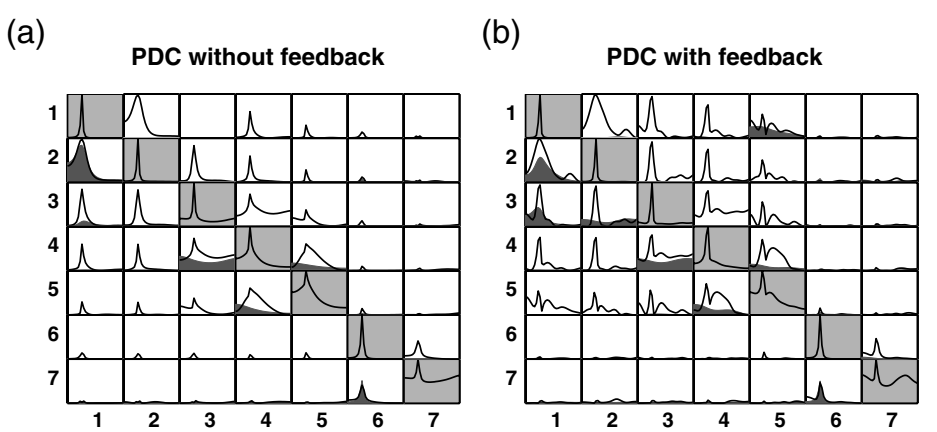

Fig. 7. Estimated PDC for Model I without (a) and with (b) feedback from $x_5(n)$ to $x_1(n)$ using 500 simulated points. Note how $x_6(n)$ and $x_7(n)$ show residual classical coherence with the other time series, despite their lack of direct connection.

where $x_1(n)$ is an oscillator driving, directly or indirectly, all the other structures. In this emulation, the odd numbered signals represent the left hemisphere leaving the other ones to map the other hemisphere as in Fig. 9. An example of the simulated signals is portrayed in Fig. 10.

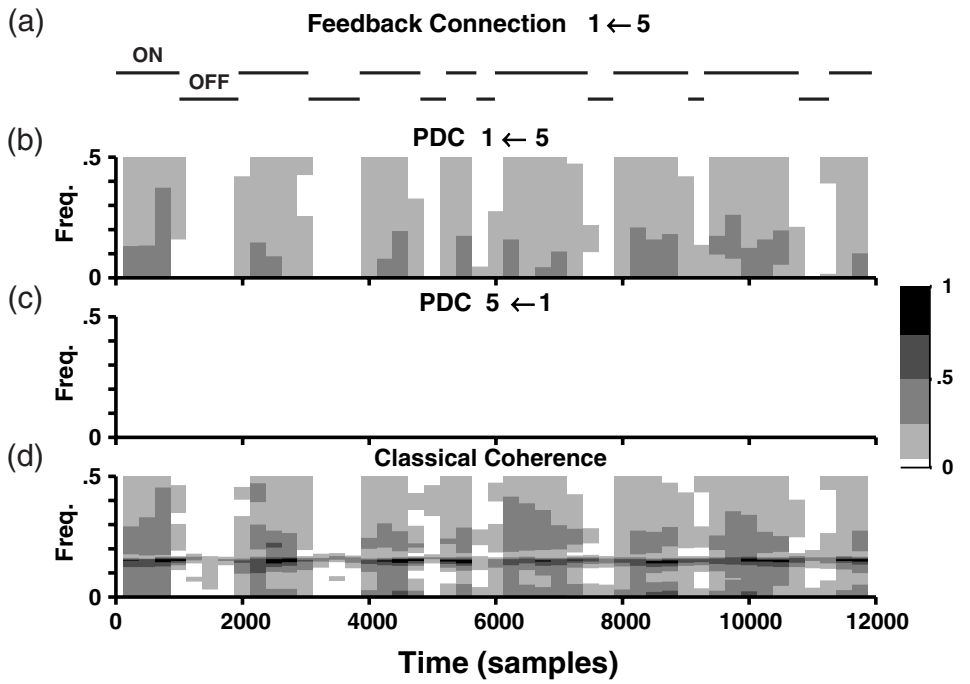

Fig. 8. Gray scale plots show the time evolution of the PDC (b and c) and classical coherence (d) between structures 1 and 5 calculated from 250 simulated data point segments (overlapping by 50%) as the feedback from $x_5(n)$ and $x_1(n)$ in Model I is switched on and off (a). The evolution of the classical coherence between these structures is also shown (d).

DTF results are shown in Fig. 11a together with its corresponding inferred signal flow graph in Fig. 11c. Note that DTF correctly identifies $x_1(n)$ as the source driving all other structures (this is the basis of DTF's success as an identifier of epileptic foci in Franaszczuk et al. (1994)). As in the previous example, however, DTF remains ambiguous as to the pathway actually followed by the signal. These possible signal pathway alternatives turn out resolved in a much simpler fashion by examining PDC in Fig. 11b which leads to a correct signal flow graph (Fig. 11d).

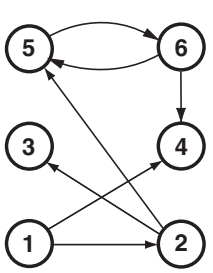

Fig. 9. Signal flow diagram for Model II.

Matching PDC calculations using simulated rather than theoretical values are shown in Fig. 12. According to PDC, $x_1(n)$'s role as a signal source for the whole structure is equally well deducible.

A question that can arise about the use of PDC regards what happens when calculations are based on the processing of a reduced number of structures than are actually representative of the structure and dynamics of the process. Suppose we want to infer the direct interhemispheric influence by looking only at pairs of signals from both hemispheres along the sagittal plane, i.e. by computing the pairwise PDC of the pairs like $(x_1(n), x_2(n))$, $(x_3(n), x_4(n))$ and $(x_5(n), x_6(n))$ without making joint calculations involving the other structures.

The results of these separate pairwise analyses are shown in Fig. 13c, 13b and 13a, respectively. In the presence of actual connections as for Fig. 13a,c, their mutual feedback is correctly deduced from simulated data, as opposed to the relationship between $x_3(n)$ and $x_4(n)$, where feedback presence is incorrectly detected despite the absence of an actual direct inter-

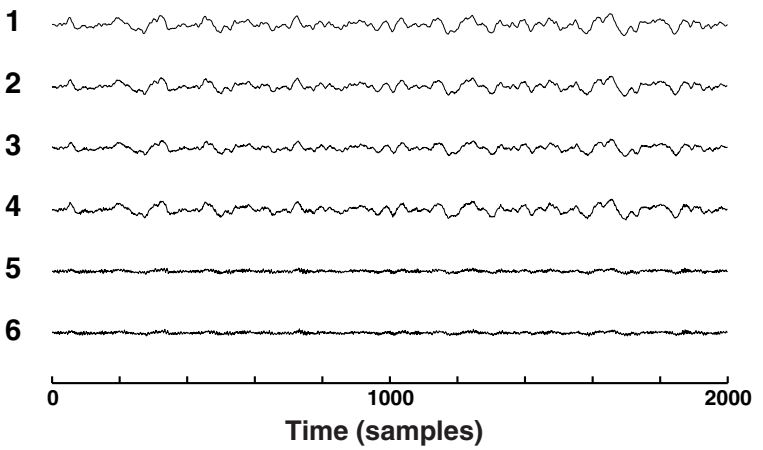

Fig. 10. Signals obtained by simulating Model II.

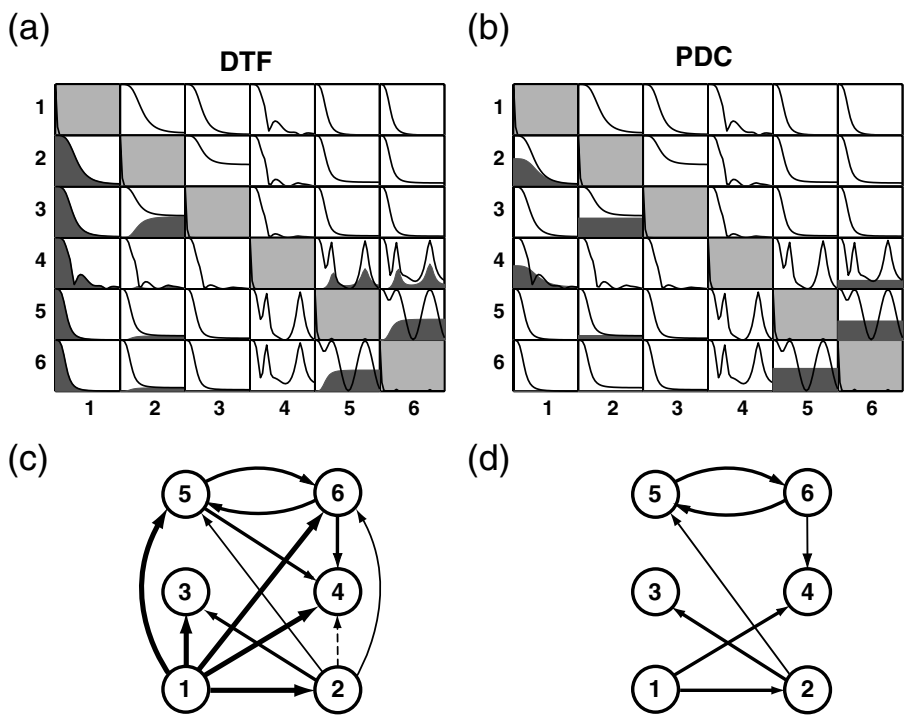

Fig. 11. Comparison between the theoretical DTF (a) (and its inferred structural interactions (c)) and the theoretical PDC results (b) (with its signal flow graph (d)). Spectral densities for the time series are depicted along the shaded main diagonal of the array. The pairwise classical coherences (solid lines) are also shown. In the signal flow graphs (c) and (d), connection arrow thickness is drawn proportional to the magnitude of DTF or PDC. Note that signal power is confined to lower frequencies.

connection. This means that we must not leave out signals from essential structures while performing the joint simultaneous signal analysis for functional structure inference.

The only hope for understanding the relationships among diverse neural structures lies in the processing of a representative number of signals simultaneously.

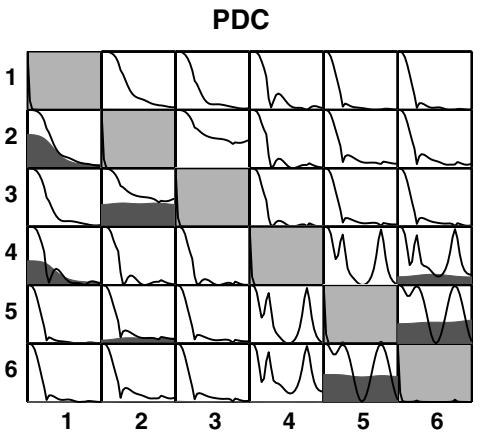

Fig. 12. Estimated PDC for Model II using 500 simulated data points.

An application to experimental data

We illustrate PDC in connection to local field potentials recorded from a rat in exploratory behavior. The simultaneously processed structures comprise the hippocampal CA1 field, somatosensory (A3) and motor (A10) cortical areas and the dorsal raphe (DR), where rhythmic oscillations in the theta range are observed during desynchronized sleep and alert states. Detailed DTF analysis of the same record of these four jointly processed structures appeared in Baccalá et al. (1998) with special attention to the relationship between CA1 and A3. Fig. 14 depicts the PDC time evolution between these structures using the electromyogram from neck muscles to label behavioral states. For the first 30 s of this recording segment, the rat actively explored a lighted cage, then gradually turned inactive as can be followed by electromyogram. Around 52 s, the rat resumed the exploratory behavior when the cage lights were turned off. As attested by looking at classical coherence and recording traces of Figs. 15 and 16, rhythmic oscillations are more prominent during active exploratory behavior.

In choosing special episodes in this record we consider the period lasting between 18 and 20 s (Fig. 15a) as characterized by high-amplitude electromyographic activity of neck muscles. The main feature of the DTF's interactions (Fig. 15b) results in the fully connected graph (Fig. 15d) that portrays the active participation of all structures. PDC (Fig. 15c) reveals the underlying signal feedback pattern (two-way interactions) and highlights DR's possibly important role. A drastically different picture emerges for the segment between 48 and 50 s of this same record (Fig. 16a) when the animal's neck muscles show low activity. DTF interactions (Fig. 16b) pro-

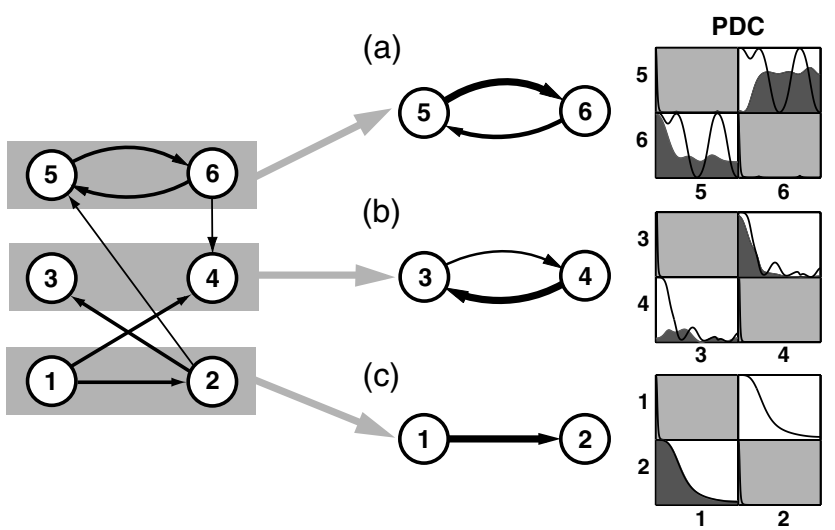

Fig. 13. PDC results of processing pairwise structures (5,6) (a), (3,4) (b), and (1,2) (a) representing opposite hemispheres in Model II that show the possibility of incorrect structural inference for the pair (3,4) (b) when not all the structures relevant to the dynamics of the model are considered jointly.

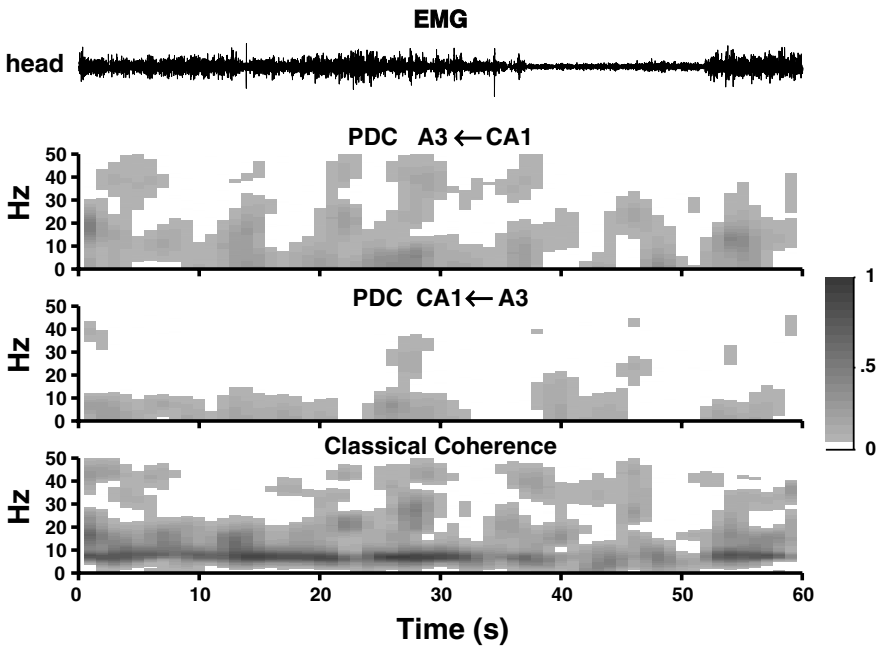

Fig. 14. Time evolution of the PDC analysis highlighting the relationship between A3 and CA1 for a rat whose exploratory behavior is labelled via the electromyogram (EMG) from its neck muscles. A gray scale is used to represent the magnitude of PDC and classical coherence. The corresponding time evolution of the DTF between these structures appeared in Baccalá et al. (1998).

duce a more sparsely connected graph (Fig. 16d) as characterized by fewer strong connections. In comparing PDC calculations Fig. 15c,e against Fig. 16c,e one notices DR's role of reversal switching from being predominantly a source to being an information sink. Furthermore, note how the influence of CA1 over DR is essentially indirect with the signal first flowing through A3 and A10 in Fig. 16e, in sharp contrast to the PDC functional connectivity graph corresponding to the exploratory behavior segment (Fig. 15e), where all structures receive substantial influence from dorsal raphe (DR). Also in the quiet state (Fig. 16e), information is mostly being relayed from the other structures through A10 to DR. This example highlights the distinct and potentially interesting functional connectivity patterns that characterize different behavioral states.

Conclusions and comments

By analyzing linear toy models, we show PDC's superior performance over other commonly used methods specially cross-correlation and classical coherence, while DTF analysis provides complementary information whose analysis is less clear than PDC's. The main advantage of PDC lies in the graphically unambiguous frequency domain display of the relationships among simultaneous measurements of several time series as PDC can clearly expose the feedback structure between directly connected pairs of neural elements provided all the structures representative of the dynamics are jointly processed.

Simultaneous recordings as well as the analysis of representative samples of neural elements through multi-site multichannel recording is therefore crucial for deducing functional connectivity. This acquires special importance in view of the fact that even PDC pairwise analysis may induce misleading conclusions about the nature of the interaction among neural elements. We therefore conclude that the use of techniques based on the processing pairwise time series are doomed to failure and that only the processing of many simultaneous structures can lead to an understanding of neural ensemble information processing and coding.

Though unaddressed in this paper, statistical issues are important. While asymptotic results for the $a_{ij}(r)$ coefficients exist and lead to Granger causality

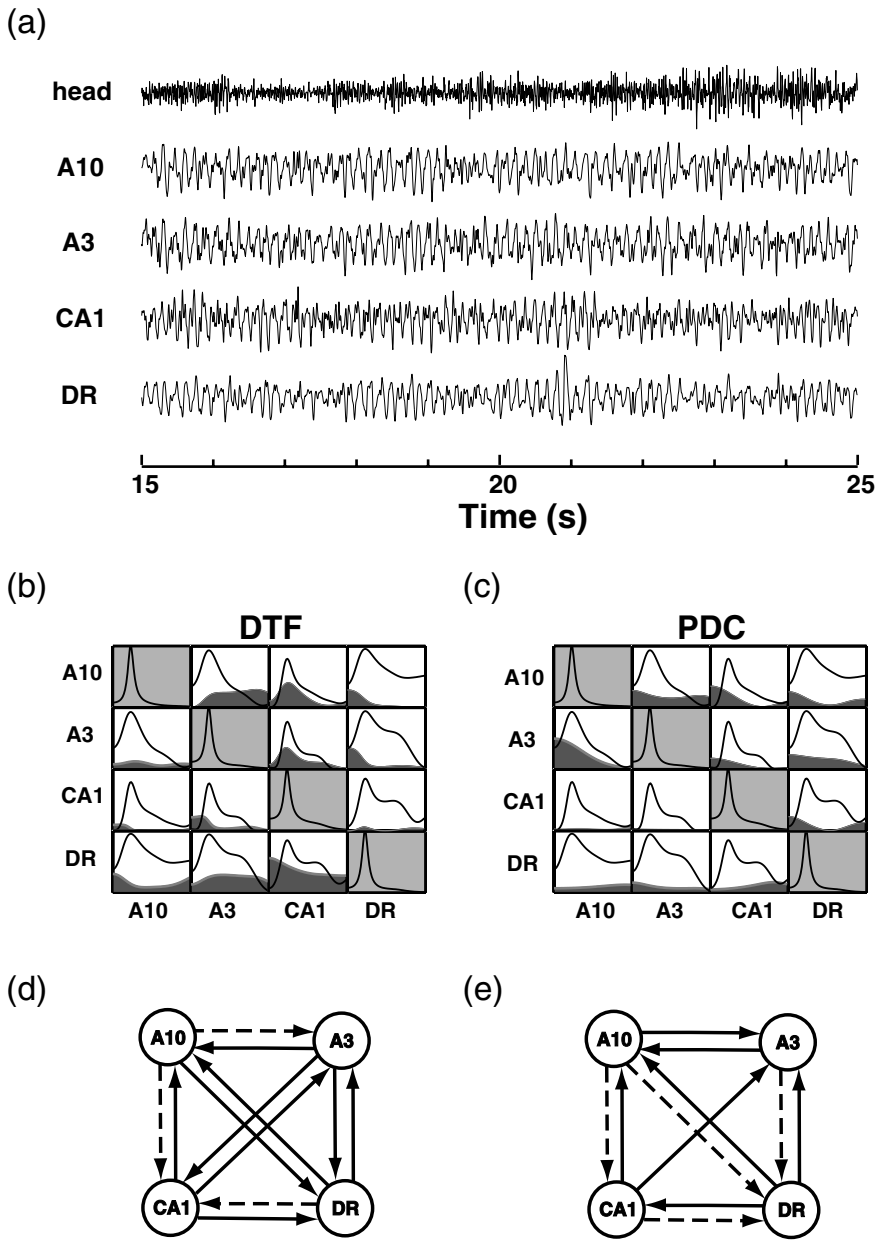

Fig. 15. Ten-second-long segment recording (corresponding to the segment 15–25 s of Fig. 14, sampled at 256 Hz) (a) from a rat engaged in active exploratory behavior. The upper trace (head) is the electromyogram from neck muscles; the other four traces are local field potentials showing rhythmic theta oscillations recorded from motor (A10) and somatosensory (A3) cortices, hippocampus (CA1) and dorsal raphe (DR). The DTFs (b) determined from segment 18–20 s show strong functional connectivity between most of the structures; weaker directional information flow occurs for the pairs DR → CA1, A10 → CA1 and A10 → A3. In (d) arrows indicate the direction of information flow resulting from DTF analysis; the weaker DTFs are indicated by dashed lines. Matching PDC analysis results (c) from the same segment lead to the functional connectivity graph (e) which shows that DR not only sends but also receives information from the other structures. As in (d), weak PDC values are represented by dashed arrow (pairs A10 → DR, A10 → CA1, A3 → DR, and CA1 → DR). In all plots in (b) and (c), the x-axis represents the frequency in the range 0–32 Hz, while the y-axis for power spectrum plots is scaled between 0 and peak value, and values for the other coherence plots lie between 0 and 1.

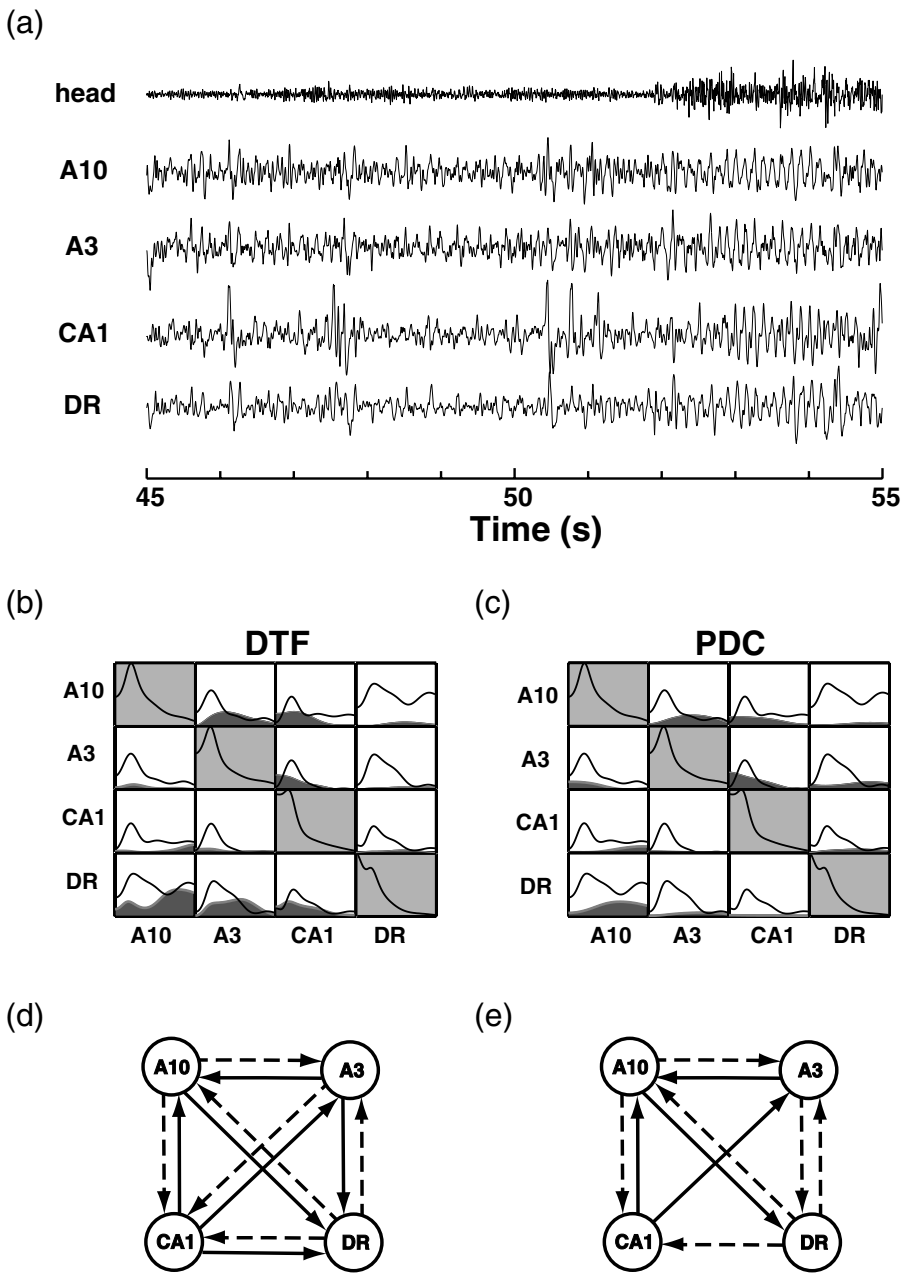

Fig. 16. Ten-second-long recording segment (a) (corresponding to the 45–55 s behavioral segment of Fig. 14, sampled at 256 Hz) showing the transition from the quiet state to active exploratory behavior induced by turning lights off at around 52 s. See Fig. 15 for details on channel labels. Note that theta waves become prominent in all four brain structures concomitantly with the onset of electromyographic activity. When compared to Fig. 15d, DTFs determined from segment 48–50 s (b) shows a larger number of weaker functional connections (d) indicated by dashed arrows. The corresponding PDC analysis (c) and its functional connectivity graph (e) portray weaker connectivity from DR to all other structures. During this episode the DTF graph connectivities (d), CA1 → DR and A3 → DR are not matched by direct connections in the PDC graph (e). They can, however, be explained respectively by the existence of indirect signal pathways CA1 → A10 → DR and A3 → A10 → DR. Note also that DR is essentially an information sink while CA1 is mainly an information source. In all plots in (b) and (c), the x-axis represents the frequency in the 0 to 32 Hz range, while the y-axis for power spectrum plots is scaled between 0 and peak value, and for coherence plots between 0 and 1.

tests (Lutkepohl, 1993; Baccalá et al., 1998), their usefulness is less clear because of the 'quasi-stationary' nature of neural signals. More importantly perhaps, as our examples show, is the fact that weak connections can be barely detectable. This is specially true in the case of DTF where the effect of weakly connected signal pathways is compounded (for example see Fig. 6a,c). Also, the number of simultaneously processed structures affects the achievable temporal resolution as more data points become necessary to insure statistically reliable detection of weak connections.

Finally, it is important to have in mind that, though based on linear time series modelling, PDC proves applicable and useful for the analysis of multiple structures that involve some levels of nonlinear interactions as discussed in Sameshima and Baccalá (1999). In fact, to our knowledge, PDC is the only existing practical method that effectively goes beyond pairwise analysis and is capable of efficiently handling multiple structures simultaneously as is essential for reliable functional structural inference.

Acknowledgements

This work received financial support from CNPq, PRONEX and FAPESP grants to the authors.

Appendix A

If $\boldsymbol{x}_i(n)$, $1 \leq i \leq N$, represent simultaneously processed discrete time signals, the canonical way to represent the relationship between these time series in the frequency domain is via their joint power spectral density matrix, which reads

$$\boldsymbol{S}(f) = \begin{bmatrix} S_1(f) & S_{12}(f) & S_{13}(f) \\ S_{21}(f) & S_2(f) & S_{23}(f) \\ S_{31}(f) & S_{32}(f) & S_3(f) \end{bmatrix} \tag{6}$$

in a $N = 3$ example. In general, one may calculate $\boldsymbol{S}(f)$ by using a multivariate (vector) autoregressive model (Priestley, 1981; Lutkepohl, 1993)

$$\begin{bmatrix} x_1(n) \\ \vdots \\ x_N(n) \end{bmatrix} = \sum_{r=1}^{p} \boldsymbol{A}_r \begin{bmatrix} x_1(n-r) \\ \vdots \\ x_N(n-r) \end{bmatrix} + \begin{bmatrix} w_1(n) \\ \vdots \\ w_N(n) \end{bmatrix} \tag{7}$$

with $w_i(n)$ standing for white uncorrelated innovation noises. The coefficient matrices $\boldsymbol{A}_r$, for each lag r, may be estimated either using least squares or fast maximum entropy methods. The appropriate order of the model p can be inferred using Akaike's *AIC* criterion (Marple, 1987). In this case, the power spectral density matrix may be written as

$$\boldsymbol{S}(f) = \boldsymbol{H}(f)\boldsymbol{\Sigma}\boldsymbol{H}^H(f) \tag{8}$$

where

$$\boldsymbol{\Sigma} = \begin{bmatrix} \sigma_{11}^2 & \dots & \sigma_{1N} \\ \vdots & \ddots & \vdots \\ \sigma_{N1} & \dots & \sigma_{NN}^2 \end{bmatrix} \tag{9}$$

is the covariance matrix of $w_i(n)$, and

$$\boldsymbol{H}(f) = \bar{\boldsymbol{A}}^{-1}(f) = (\boldsymbol{I} - \boldsymbol{A}(f))^{-1} \tag{10}$$

with

$$\boldsymbol{A}(f) = \sum_{r=1}^{p} \boldsymbol{A}_r z^{-r} \Big|_{z=e^{-j2\pi f}}$$

At this point, one option for describing the mutual interaction between pairs of time series may be obtained through a generalized definition of the *directed coherence* from j to i as (Baccalá and Sameshima, 1998; Baccalá and Sameshima, 1999)

$$\gamma_{ij}(f) = \frac{\sigma_{jj} H_{ij}(f)}{\sqrt{S_i(f)}}, \tag{11}$$

where

$$S_i(f) = \sum_{j=1}^{N} \sigma_{jj}^2 \left| H_{ij}(f) \right|^2. \tag{12}$$

Remark 1 *The definition of DTF in Franaszczuk et al. (1994) is a special case where σ_{ii} are made equal to 1 in Eq. 11. Because of its relationship to the power spectral density matrix, $\left|\gamma_{ij}(f)\right|$ may be interpreted as a fraction of the power originating in $x_j(n)$ that reaches $x_i(n)$.*

An alternative way to describe the mutual interaction is via the $a_{ij}(r)$ elements of $\boldsymbol{A}_r$, i.e. by testing Granger causality directly. If $\bar{a}_{ij}(f)$ be $\bar{\boldsymbol{A}}(f)$'s i, j-th element, i.e. the i-th component of the j-th column $\bar{\boldsymbol{a}}_j(f)$ of $\bar{\boldsymbol{A}}(f)$. After suitable normalization, discussed elsewhere (Baccalá and Sameshima, 1999), one possible definition for *partial directed coherence* is

$$\pi_{ij}(f) = \frac{\bar{a}_{ij}(f)}{\sqrt{\bar{\boldsymbol{a}}_j(f)^H \bar{\boldsymbol{a}}_j(f)}} \tag{13}$$

Remark 2 *This name, 'partial directed coherence', comes from an interpretation of $\pi_{ij}(f)$ as factor in the partial coherence $\kappa_{ij}(f)$ between two time series (Bendat and Piersol, 1986; Baccalá and Sameshima, 1999).*

Remark 3 *The relationship between PDC and DTF is that they are based, respectively, on the matrices $\bar{\boldsymbol{A}}(f)$ and $\boldsymbol{H}(f)$ which are inverses of one another. This inverse matrix relationship occurs in graph theory where a matrix like $\bar{\boldsymbol{A}}(f)$ describes the connections of directed graphs while a matrix like $\boldsymbol{H}(f)$ is analogous to the graph reachability matrix which records the graph structures reachable from a given node (Baccalá et al., 1991).*

Remark 4 *When $N = 2$, PDC leads exactly to the same estimator as DTF (Baccalá and Sameshima, 1999).*

References

Arnhold, J., Grassberger, P., Lehnertz, K. and Elger, C.E. (1999) A robust method for detecting interdependencies: application to intracranially recorded EEG. *Physica D*, 134: 419–430.

Baccalá, L.A. and Sameshima, K. (1998) Directed Coherence: A tool for exploring functional interactions among brain structures. In: M.A.L. Nicolelis (Ed.), *Methods for Neural Ensemble Recordings*. CRC Press, Boca Raton, FL, pp. 179–192.

Baccalá, L.A. and Sameshima, K. (2001) Partial directed coherence a new concept in neural structure determination. *Biol. Cybern*., 84: 463-474.

Baccalá, L., Nicolelis, M., Yu, C. and Oshiro, M. (1991) Structural analysis of neural circuits using the theory of directed graphs. *Comp. Biomed. Res.*, 24: 7–28.

Baccalá, L.A., Sameshima, K., Ballester, G., Valle, A.C. and Timo-Iaria, C. (1998) Studying the interaction between brain structures via directed coherence and Granger causality. *Appl. Sig. Process.*, 5: 40–48.

Bendat, J.S. and Piersol, A.G. (1986) *Random Data: Analysis and Measurement Procedures*. John Wiley, New York, 2nd ed.

Brunel, N. and Nadal, J.P. (1998) Mutual information, Fisher information, and population coding. *Neural Comput.*, 10: 1731–1757.

Christakos, C.N. (1997) On the detection and measurement of synchrony in neural populations by coherence analysis. *J. Neurophysiol.*, 78: 3453–3459.

Duckrow, R.B. and Spencer, S.S. (1992) Regional coherence and the transfer of ictal activity during seizure onset in the medial temporal lobe. *Electroencephalogr. Clin. Neurophysiol.*, 82: 415–422.

Eichenbaum, H.B. and Davis, J.L. (Eds.) (1998) *Neuronal Ensembles: Strategies for Recording and Decoding*. John Wiley, New York.

Franaszczuk, P.J., Bergey, G.K. and Kaminski, M.J. (1994) Analysis of mesial temporal seizure onset and propagation using the directed transfer function method. *Electroencephalogr. Clin. Neurophysiol.*, 91: 413–427.

Glaser, E. and Ruchkin, D. (1976) *Principles of Neurobiological Signal Analysis*. Academic Press, New York.

Granger, C.W.J. (1969) Investigating causal relations by econometric models and cross-spectral methods. *Econometrica*, 37: 424–438.

Lutkepohl, H. (1993) *Introduction to Multiple Time Series Analysis*. Springer, Berlin, 2nd ed.

Marple, S.L., Jr. (1987) *Digital Spectral Analysis*. Prentice-Hall, Englewood Cliffs, NJ.

Nicolelis, M.A.L. (Ed.) (1998) *Methods for Neural Ensemble Recordings*. CRC Press, Boca Raton, FL.

Priestley, M.B. (1981) *Spectral Analysis and Time Series*. Academic Press, London.

Rieke, F., Warland, D., de Ruyter van Steveninck, R. and Bialek, W. (1997) *Spikes: Exploring the Neural Code*. MIT Press, Cambridge, MA.

Rosenberg, J., Halliday, D., Breeze, P. and Conway, B. (1998) Identi c ation of patterns of neuronal connectivity — partial spectra, partial coherence, and neuronal interactions. *J. Neurosci. Methods*, 83: 57–72.

Saito, Y. and Harashima, H. (1981) Tracking of information within multichannel EEG record — causal analysis in EEG. In: N. Yamaguchi and K. Fujisawa (Eds.), *Recent Advances in EEG and EMG Data Processing*. Elsevier, Amsterdam, pp. 133–146.

Sameshima, K. and Baccalá, L. (1999) Using partial directed coherence to describe neuronal ensemble interactions. *J. Neurosci. Methods*, 94: 93–103.

Schiff, S.J., So, P., Chang, T., Burke, R.E. and Sauer, T. (1996) Detecting dynamical interdependence and generalized synchrony through mutual prediction in a neural ensemble. *Phys. Rev. E*, 54: 6708–6724.

Schnider, S.M., Kwong, R.H., Lenz, F.A. and Kwan, H.C. (1989) Detection of feedback in the central nervous system using system identi c ation techniques. *Biol. Cybern.*, 60: 203–212.

Yamada, S., Nakashima, M., Matsumoto, K. and Shiono, S. (1993) Information theoretic analysis of action potential trains, I. Analysis of correlation between 2 neurons. *Biol. Cybern.*, 68: 215–220.